JAERI-M
84-193

MONTE CARLO CALCULATION OF THE CHARACTERISTICS OF SOURCE NEUTRONS AND IRRADIATION FIELD OF THE FNS ROTATING TARGET

October 1984

Yasushi SEKI, Yujiro IKEDA, Yukio OYAMA,
Tomoo NAKAMURA, Hiroshi MAEKAWA,
Hiromitsu KAWASAKI* and Koubun YAMADA*

日本原子力研究所
Japan Atomic Energy Research Institute

JAERI-Mレポートは，日本原子力研究所が不定期に公刊している研究報告書です。

入手の問合わせは，日本原子力研究所技術情報部情報資料課（〒319－11茨城県那珂郡東海村）あて，お申しこしください。なお，このほかに財団法人原子力弘済会資料センター（〒319-11茨城県那珂郡東海村日本原子力研究所内）で複写による実費頒布をおこなっております。

JAERI-M reports are issued irregularly.

Inquiries about availability of the reports should be addressed to Information Division, Department of Technical Information, Japan Atomic Energy Research Institute, Tokai-mura, Naka-gun, Ibaraki-ken 319-11, Japan.

編集兼発行　日本原子力研究所
印　　刷　日立高速印刷株式会社

JAERI-M 84-193

Monte Carlo Calculation of the Characteristics of Source Neutrons and Irradiation Field of the FNS Rotating Target

Yasushi SEKI, Yujiro IKEDA, Yukio OYAMA, Tomoo NAKAMURA, Hiroshi MAEKAWA, Hiromitsu KAWASAKI* and Koubun YAMADA*

Department of Reactor Engineering,
Tokai Research Establishment, JAERI

(Received September 28, 1984)

The characteristics of the source neutrons generated by the rotating target and the irradiation field in the target room at the Fusion Neutronics Source (FNS) were calculated using a three-dimensional Monte Carlo method. The angular distributions of reaction rates around the target, the radial distribution of reaction rates in the target room and the source neutron spectrum were calculated and compared with the measured results. The comparison showed a reasonably good agreement for all the reaction rates and source neutron spectrum. The good agreement assures the validity of the calculated source neutron characteristics to be used in the future analyses of the experiments using the same rotating target.

Keywords: Monte Carlo Method, Source Neutron Characteristics, Irradiation Field Characterization, D-T Neutron, Rotating Target, Energy Spectrum, Angular Distribution, Activation Foil, TOF Method

---

* Century Research Center Cooperation

ＦＮＳ回転ターゲットの中性子源特性および照射場特性のモンテカルロ計算

日本原子力研究所東海研究所原子炉工学部
関　　泰・池田裕二郎・大山　幸夫・中村　知夫
前川　　洋・川崎　弘光*・山田　光文*

（１９８４年９月２８日受理）

ＦＮＳ（Fusion Neutronics Source）における回転ターゲットから生成される源中性子およびターゲット室の照射場の特性を，３次元モンテカルロ法を用いて計算した。反応率のターゲット周囲の角度分布，反応率のターゲット室内の径方向分布と源中性子スペクトルを計算して実験結果と比較した。その結果全ての反応率と源中性子スペクトルについて計算と実験の良い一致が得られた。この良い一致は，計算された中性子源特性が将来のこの回転ターゲットを用いた実験の解析に適用するにふさわしいものであることを示している。

＊　センチュリー・リサーチ・センター（株）

CONTENTS

目　　次

1. INTRODUCTION

A rotating target is being used in a series of fusion reactor neutronics experiments conducted in the Fusion Neutronics Source (FNS) in the Japan Atomic Energy Research Institute (JAERI)[1]. It is essential for the analysis and interpretation of the experiments to obtain the accurate information of the characteristics of the source neutrons and the irradiation field[2]-[7]. The source neutron characteristics are dependent on the neutron generation scheme, i.e. the configuration of the rotating target, target cooling method, etc. The irradiation field characteristics depend not only on the source neutron characteristics but also on neutrons reflected by the room wall and the fixture in the room.

In order to determine these characteristics, the angular distribution of the neutron flux around the target, the spatial distribution of neutrons in the room, and the source neutron energy spectrum at 80° to the deuteron beamline have been measured with activation foils, fission chambers and NE 213 scintillation detectors.[8]

A Monte Carlo calculation of the source neutron characteristics of the rotating target and neutron distribution in the experiment room was conducted to reinforce and supplement the measured results. At the same time, the applicability of the Monte Carlo calculation method was examined. The Monte Carlo calculation method which had proved to be satisfactory in obtaining the source neutron characteristics of a water cooled target[7] was used.

Although the further measurements to determine the characteristics of source neutron and irradiation field have been performed[9], the present calculations are for the measurements conducted prior to the August of 1983.

2. CALCULATIONAL MODEL AND METHODS

2.1 Calculational Model of the Target Assembly and Experiment Room

The vertical cross-sectional view of the rotating target assembly is shown in Fig. 1. A 2.5 mg/cm^2 thick titanium-tritide (Ti-T) is coated on the spherical plate made of 0.8 mm* thick AMZIRC (Zr 0.15 % Cu). The target is cooled with water which flows through the 2 mm gap between the AMZIRC plate and the outer plate made of 0.8 mm thick 304 SS. More detailed configurations of the cover and the cone section of the target assembly including their dimensions are shown in Figs. 2 and 3, respectively. The actual configuration of the copper (Cu) collimator is shown in Fig. 4. The collimator is modelled as a portion of a cone made of a mixture of Cu(30 %) + H_2O(42 %) + SS(8 %). The AMZIRC target rotates around the axis of the cone section. The target also swings in the vertical direction so as to utilize the wide circular band of the coated T on the plate.

Based on the figures and the drawings of the target room, the calculational model of the target and the room was made using the general geometry package of the Monte Carlo neutron transport code MORSE-GG[10]. The calculational model of the target is shown in Fig. 5a and 5b, which were drawn with the TOPIC code[11] for checking the geometry treated by the MORSE-GG code. The vertical position of the target is assumed to be at the middle point of the swinging motion.

Figure 6 shows the vertical cross sectional view of the target and the room at the surface along the deuteron beamline. The beam spot is at 1.8 m above the floor, 2.7 m below the ceiling and 2.5 m from the 4 side walls. Although 2 cm thick mortar is coated on the side walls, the mortar is neglected in the present calculational

* After this report was written, the thickness of the AMZIRC plate was found to be in the range of 0.90-0.92 mm. The thickness increase of 0.1 mm will reduce the source neutrons by only 0.5% in the 80° direction to the beamline.

model. Figure 7 shows the horizontal cross section of the target room. At the 80° direction to the beamline, there is an experimental hole about 70 cm in diameter in the concrete wall 2.5 m thick.

Atomic densities of the materials used in the calculational models of the target assembly and the experiment room are summarized in Table 1.

2.2 Source Generation Method

Source neutrons were generated taking account of the kinematics of a two-body reaction and the energy loss of deuteron in a Ti-T thick target.[4] The neutrons were emitted from a 2 cm diameter beam spot on the surface of the rotating target assuming a Gaussian distribution in the radial direction with the peak at the center of the spot. The energy E_1 of the deuteron causing the D-T reaction in the Ti-T thick target was determined from the data in Ref. 4.

The anisotropy of neutron emission in the center of mass system has been taken into consideration utilizing the representation of the angular dependence in Ref. 5, i.e.,

$$\frac{\sigma_n(\theta)}{\sigma_n(0)} = 0.998 + 0.0213\cos\theta_n - 0.0190\cos^2\theta_n \qquad (1)$$

for the bombarding energy of 350 keV, which is nearly the same as that of 300 keV in FNS rotating target. In Eq. (1), $\sigma_n(\theta)/\sigma_n(0)$ is the ratio of the differential cross sections of neutrons from the D-T reaction emitted in the angle θ_n over that emitted in the deuteron beam direction

After E_1 and θ_n were determined, the emission angle ϕ_n in the laboratory system was obtained by the following equation derived from Ref. 4:

$$\sin\phi_n = \pm \frac{\sin\theta_n}{\sqrt{1 + 2\gamma\cos\theta_n + \gamma^2}} \quad , \qquad (2)$$

where

$$\frac{1}{\gamma^2} = \frac{m_\alpha}{m_n} \frac{(m_1 + m_2)}{m_1} \left[\frac{m_2}{m_1 + m_2} + \frac{Q}{E_1} \right] ,$$

m_1 = mass of deuteron,

m_2 = mass of triton,

m_n = mass of neutron,

m_α = mass of alpha particle,

E_1 = incident energy of deuteron,

Q = 17.6 MeV

After determining ϕ_n, the kinetic energy of neutron was obtained from the following equations[12] based on the Relativistic Theory:

$$E_L(E_1, \phi_n) = W_n - m_n , \tag{3}$$

where MeV unit is used both for energy and mass, and

$$W_n = \frac{1}{2} \{ b \pm \sqrt{b^2 - 4ac} \} = \text{total energy of neutron},$$

$$a = (W_1 + m_2)^2 - (W_1 - m_1^2) \cos^2 \phi_n ,$$

$$b = (m_1^2 + m_2^2 + m_n^2 - m_\alpha^2 + 2m_2 W_1)(W_1 + m_2) ,$$

$W_1 = m_1 + E_1$ = total energy of deuteron.

2.3 Radiation Transport Calculations

The Monte Carlo radiation transport code MORSE-GG[10] was used to calculate the neutron transport in the target assembly and the room. Macroscopic cross sections for the constituent materials of the target and room in the form of 28-group neutron and 7-group gamma ray (28n - 7γ) coupled cross section, were used in the calculations. The 28n - 7γ cross sections have been derived by collapsing the 135n - 21γ cross sections with the flux weight obtained by a one dimensional ANISN calculation,[13]

using a spherical model of the target assembly and the room. The 135n - 21γ coupled cross sections have been processed from the ENDF/B-4 nuclear data file[14] by the NJOY code system[15] and the GAMLEG-JR code[16] following the calculational flow shown in Fig. 8. The energy group structure of the 28n - 7γ cross sections are given in Table 2.

Source neutrons were generated in the target as described in 2.2 with the initial weight of 1.0. The histories of neutrons and secondary gamma rays were followed until either they escaped from the calculational system or their weight became smaller than specified values.

2.4 Detector Estimators

Two types of detector estimators, namely the track length estimator and the point detector estimator, were used to obtain the required quantities efficiently. The former is suited to obtain uncollided source neutron flux and the activation reaction rates that are induced mainly by uncollided source neutrons. The latter is appropriate in deriving collided neutron flux and gamma ray flux. From comparison of the results using the two types of detectors, the adequacy of both methods was ensured. In the point detector method, a modified SDATA subroutine was used to calculate the uncollided flux contribution from the anisotropic distributed source to the point detectors.

In the calculation with the track length estimators, about 860 thousand source neutrons were generated to obtain the reaction rates within the statistical error less than about 0.02 fsd (fractional standard deviation). The required CPU (central processing unit) time using the FACOM M-200 computer was about 5 hours.

On the other hand, about 105 thousand histories of source neutrons were followed to obtain the radial distribution of reaction rates within

the accuracy of about 0.02 fsd, using 5 point detectors. This took about 1 hour of the CPU time.

3. CALCULATED RESULTS AND COMPARISON WITH EXPERIMENT

3.1 Angular Distribution of Reaction Rates

Angular distribution of neutrons around the target was measured using the activation foils and fission chambers. The angular distribution of ^{232}Th fission rate measured at 1.5 m from the neutron generation point is shown in Fig. 9. The open circles show the measured values. The calculated values obtained using the track length estimator (TL) method are shown with black triangles. Closed circles denote the calculated values obtained with the point detector (PD) method. Measured and calculated results agree very well except at -135°. Neutrons at this direction were shielded by a motor located in this direction, which was not included in the calculational model. The calculated values obtained with the TL method and those with the PD method agree each other within the statistical errors. The statistical errors of the calculated values for the same 60 min computation time are 8-10 % for the TL method and less than 2.4 % for the PD method. The good agreement obtained between the TL method and PD method suggests the applicability of the PD method to the reaction rate calculations at the locations far from the source where it is difficult to make statistical errors sufficiently small with the TL method.

Angular distribution of neutrons around the source was measured using the activation foils in the holizontal plane at the radius R = 30 cm from the source. The cross sections of the activation reactions used in the measurements are shown in Figs. 10a and 10b. These cross sections have been obtained from Ref. (17) and (18).

The measured angular distributions of $^{58}Ni(n,2n)^{57}Ni$, $^{93}Nb(n,2n)^{92m}Nb$, $^{197}Au(n,2n)^{196}Au$, $^{27}Al(n,\alpha)^{24}Na$, $^{56}Fe(n,p)^{56}Mn$ and $^{197}Au(n,\gamma)^{198}Au$ are

compared with the calculated ones using the TL method in Figs. 11-16. The effective threshold energies of the reactions except the exothermic $^{197}Au(n,\gamma)^{198}Au$ reaction are listed in the figures.

In the case of the $^{58}Ni(n,2n)^{57}Ni$ reaction rate, the calculated value at 0° is about 20 % smaller than the measured one. When the recently measured cross section of the reaction[19] is used in place of the cross section in the ENDF/B-V dosimetry file, the calculated results are found to agree well with the measured ones[20].

The calculations and measurements are in good agreement for the reactions $^{93}Nb(n,2n)^{92m}Nb$, $^{197}Au(n,2n)^{196}Au$, $^{27}Al(n,\alpha)^{24}Na$ and $^{56}Fe(n,p)^{56}Mn$. The statistical errors in the calculated $^{197}Au(n,\gamma)^{198}Au$ values obtained with the TL method are too large to say anything definite about the agreement with the measured values. However, the value at 0° obtained with the PD method indicates that the calculation underestimates the measurement by ~20 %.

3.2 Radial Distribution of Reaction Rates in the 0° Direction

Radial distributions of neutrons in the 0° direction to the deuteron beam line were measured from the source generation point to the concrete room wall. The measurement used the activation foils of the $^{58}Ni(n,2n)^{57}Ni$, $^{27}Al(n,\alpha)^{24}Na$, $^{115}In(n,n')^{115m}In$, $^{115}In(n,\gamma)^{116}In$ and $^{197}Au(n,\gamma)^{198}Au$ reactions. These reaction rates at 6 selected points were calculated using the PD detectors. The results of the calculations are compared with those of the measurements in Figs. 17-20.

The calculation of the $^{58}Ni(n,2n)^{57}Ni$ reaction rate in Fig. 17 underestimates the measurement at 10 cm and 30 cm from the source. It overestimate the measurement near the concrete wall. The underestimations by the calculation at 10 cm and 30 cm are due to the

use of the inappropriate cross sections as described in 3.1. The overestimation near the wall is due to the self-shielding effect in the measurement. Since the foils were positioned along the straight line in extension of the beamline, the accumulated self-shielding by the foils resulted in the reduction of the measured values. The same reduction of the measured values was observed in the case of $^{27}Al(n,\alpha)^{24}Na$ in Fig. 18. When the number of the foils employed was small, a good agreement between the calculation and experiment was obtained for the $^{115}In(n,n')^{115m}In$ reaction rate as shown in Fig. 19. The distributions of the $^{115}In(n,\gamma)^{116}In$ and $^{197}Au(n,\gamma)^{198}Au$ reaction rates are almost flat in the target room. The calculated $^{115}In(n,\gamma)^{116}In$ reaction rate is in good agreement with the measured one. The calculated $^{197}Au(n,\gamma)^{198}Au$ reaction rate is about 20 ~ 30 % smaller than the measured values.

The underestimation of the calculated $^{197}Au(n,\gamma)^{198}Au$ reaction observed in Figs. 16 and 20 may be caused by the following reasons;

1. The error in the Monte Carlo calculation for treating the neutrons contributing to the $^{197}Au(n,\gamma)^{198}Au$ reaction, namely the neutrons with energy ~ 7 eV. The statistical error in the neutron flux in the range of 4.64 - 59.9 eV is less than 7 %.
2. The composition of wall concrete, especially the water content used in the calculation may be fairly different from the actual one with 2 cm thick mortar.

3.3 Source Neutron Spectrum at 80°

Source neutron spectrum in the 80° direction was measured using the time-of-flight (TOF) technique. Only the 80° direction measurement is possible with the TOF technique because sufficiently long flight path of 17.5 m can be obtained only through the experimental duct in the 80° direction.

The neutron spectrum in the 80° direction measured without using collimator is compared with the calculated one in Fig. 21. The measured spectrum is shown with points with error bars denoting statistical counting errors. The calculated result obtained with the calculational model including only the target assembly, is shown with a histogram. The calculated spectrum was obtained with smearing the result of a Monte Carlo calculation over the detector energy resolution function. The resolution function of the time of flight method was approximated as

$$R(E - E') = Ae^{-(E-E')^2/2\sigma^2(E)}$$

where $\sigma(E) = 0.0277\ \Delta t\ E^{3/2}/L$,

$L = 17.5$ m: Flight path,

$\Delta t = 24.44$ ns: Time resolution of pulsed D-T neutrons,

E = Neutron energy (MeV) .

A good agreement has been obtained for the source neutron peak above 9 MeV between the measurement and the calculation. The integrated counts in the peak for the measurement and calculation agree within ~4 %. At below 9 MeV for the collided neutrons, the calculation slightly underestimate the measurement. The general spectrum shape is in good agreement except for the D-D neutron peak present in the measurement. The D-D neutrons were not generated in the calculation. The slight

underestimate of the collided neutrons by the calculation is mostly due to the neutrons collided with the target room or the experimental hole side walls which were not considered in the calculation.

4. CONCLUSIONS

The characteristics of the source neutrons generated by the rotating target and the irradiation field in the target room of the FNS were calculated using a three-dimensional Monte Carlo method. The results of the calculations were compared with the measured ones and the following conclusions have been obtained.

(1) An excellent agreement was obtained in the calculated and measured angular distribution of ^{232}Th fission rate at the locations 1.5 m from the source neutron generation point. The calculated reaction rate values obtained with the point detector method and those with the track length method agreed with each other within the statistical errors. Thus the results using the point detector method were used whenever the track length method could not attain sufficiently small statistical error.

(2) Good agreements between measurement and calculation were obtained for the angular distribution of the 4 threshold reactions, namely $^{93}Nb(n,2n)^{92m}Nb$, $^{197}Au(n,2n)^{196}Au$, $^{27}Al(n,\alpha)^{24}Na$ and $^{56}Fe(n,p)^{56}Mn$.

(3) The calculated value of the $^{58}Ni(n,2n)^{57}Ni$ reaction rate at 0° to the deuteron beam was about 20 % smaller than the measured one. However, this discrepancy was resolved[20] when the recently measured cross section of this reaction[19] was employed in place of the one in ENDF/B-V dosimetry file.

(4) Considering the above cross section effect in the calculation and the self-shielding effect in the measurement, the measured and calculated radial distributions of the $^{58}Ni(n,2n)^{57}Ni$ agreed fairly well. The agreement is also good for the radial distributions of the $^{27}Al(n,\alpha)^{24}Na$ and $^{115}In(n,n')^{115m}In$ reaction rates.

(5) The measured and calculated values of the $^{115}In(n,\gamma)^{116}In$ and $^{197}Au(n,\gamma)^{198}Au$ reaction rates all showed almost flat distribution in the experimental room. The magnitude of the calculated $^{115}In(n,\gamma)^{116}In$ reaction rate was in good agreement with that of the measured one. The calculated $^{197}Au(n,\gamma)^{198}Au$ reaction rate underestimated the measured one by 20-30 %.

(6) An excellent agreement with the calculation was obtained for the source neutron energy spectrum at 80° to the beam line measured with the TOF technique. The measured and calculated source neutron peaks agreed within 4 %.

References

(1) Nakamura, T., et al.: Integral experiments on lithium oxide spherical assembly with graphite reflector and on duct streaming, Proc. 3rd IAEA Technical Committee Meeting and Workshop on Fusion Reactor Design and Technology, Tokyo, Oct. 5 16, 1981, (1982).

(2) Kuijipers, L.J.M.: Experimental model studies for fusion reactor blanket, PhD Thesis, Technische Hogeschool, Eindhoven, (1976).

(3) Perkins, L.J., et al.: Nucl. Sci. Eng., 78, 30 (1981).

(4) Benveniste, J., Zenger, J.: Information on the neutrons produced in the $^{3}H(d,n)^{4}He$ reaction, UCRL-4266, (1954).

(5) Benveniste, J., et al.: Nucl. Instrum. Methods, 7, 306 (1960).

(6) Sitaraman, S. and Woodruff, G.L.: Trans. Am. Nucl. Soc., Vol. 43, 197 (1982)

(7) Seki, Y., et al.: J. Nucl. Sci. Technol., 20 [8], 686 (1983).

(8) Ikeda, Y., et al.: to be published

(9) Oyama, Y., et al.: to be published

(10) Straker, E.A., et al.: The MORSE code — A multigroup neutron and gamma ray Monte Carlo transport code, ORNL-4585, (1970).

(11) Iida, H., Kawasaki, H.: TOPIC; A debugging code for torus geometry input data of Monte Carlo transport code, JAERI-M 8289, (in Japanese), (1979).

(12) Itoh, S.: Private communication.

(13) Engle, W.W., Jr.: A users manual for ANISN, A one-dimensional discrete ordinates transport code with anisotropic scattering, K-1693, Computing Technology Center, Union Carbide Corp. (1967).

(14) Drake, M.K. (ed.): Data formats and procedures for the ENDF neutron cross section library, BNL-50274 (T-601, TID-4500), ENDF 102, Vol. 1 (1970), revised 1974.

(15) MacFarlance, R.E., et al.: The NJOY nuclear data processing system; User's manual, LA-7584 M(ENDF-272), (1978).

(16) Miyasaka, S., et al.: GAMLEG-JR, A production code of multigroup cross sections and energy deposition coefficients for gamma-rays, JAERI-M 6936, (1977).

(17) Kinsey, R.: ENDF/B Summary Documentation, BNL-NCS-17541 (ENDF-201) 3rd Edition, ENDF/B-V, available from the National Nuclear Data Center, Brookhaven National Laboratory, Upton, N.Y. (July, 1979).

(18) Greenwood, L.R.: Extraporated Neutron Activation Cross Sections for Dosimetry to 44 MeV, ANL/FPP/TM-115 (1978).

(19) Winkler, G., et al.: Proc. Int. Conf. Nuclear Data for Science and Technology, 6-10 Sept. 1982 Antwerp.

(20) Ikeda, Y., et al.: to be published.

Table 1 Atomic densities of the materials used in the calculational models of the target assembly and the experiment room

Material	Element	Atomic density (10^{24} atoms/cm^3)
Air	O	1.13-5
	N	4.20-5
Aluminum	Al	6.004-2
Copper	Cu	8.463-2
304SS	Cr	1.741-2
	Fe	6.173-2
	Ni	8.112-3
Water	H	6.6-2
	O	3.3-2
Mild steel	Fe	8.476-2
Concrete	H	7.974-3
	C	5.409-4
	O	4.315-2
	Na	7.859-4
	Mg	3.824-4
	Al	2.637-3
	Si	1.481-2
	K	5.288-4
	Ca	2.564-3
	Fe	5.859-4

Table 2 Energy structures of the 28-group neutron and 7-group gamma ray cross sections

Neutron Energy Groups

Group No.	Lower Energy Limit (eV)	Upper Energy Limit (eV)	Group No.	Lower Energy Limit (eV)	Upper Energy Limit (eV)
1	1.583+7*	1.640+7	15	5.592+6	6.242+6
2	1.527+7	1.583+7	16	4.897+6	5.529+6
3	1.474+7	1.527+7	17	4.337+6	4.897+6
4	1.422+7	1.474+7	18	3.699+6	4.337+6
5	1.372+7	1.422+7	19	2.924+6	3.699+6
6	1.324+7	1.372+7	20	1.698+6	2.924+6
7	1.278+7	1.324+7	21	9.640+5	1.698+6
8	1.218+7	1.278+7	22	3.560+5	9.640+5
9	1.114+7	1.218+7	23	1.120+5	3.560+5
10	1.009+7	1.114+7	24	1.000+4	1.120+5
11	8.949+6	1.009+7	25	7.740+2	1.000+4
12	7.938+6	8.949+6	26	5.990+1	7.740+2
13	7.041+6	7.938+6	27	4.640+0	5.990+1
14	6.242+6	7.041+6	28	1.000-3	4.640+0

Gamma Ray Energy Groups

1	8.000+6	1.400+7
2	6.500+6	8.000+6
3	5.000+6	6.500+6
4	3.500+6	5.000+6
5	2.000+6	3.500+6
6	4.000+5	2.000+6
7	1.000-2	4.000+5

* read as 1.583×10^7

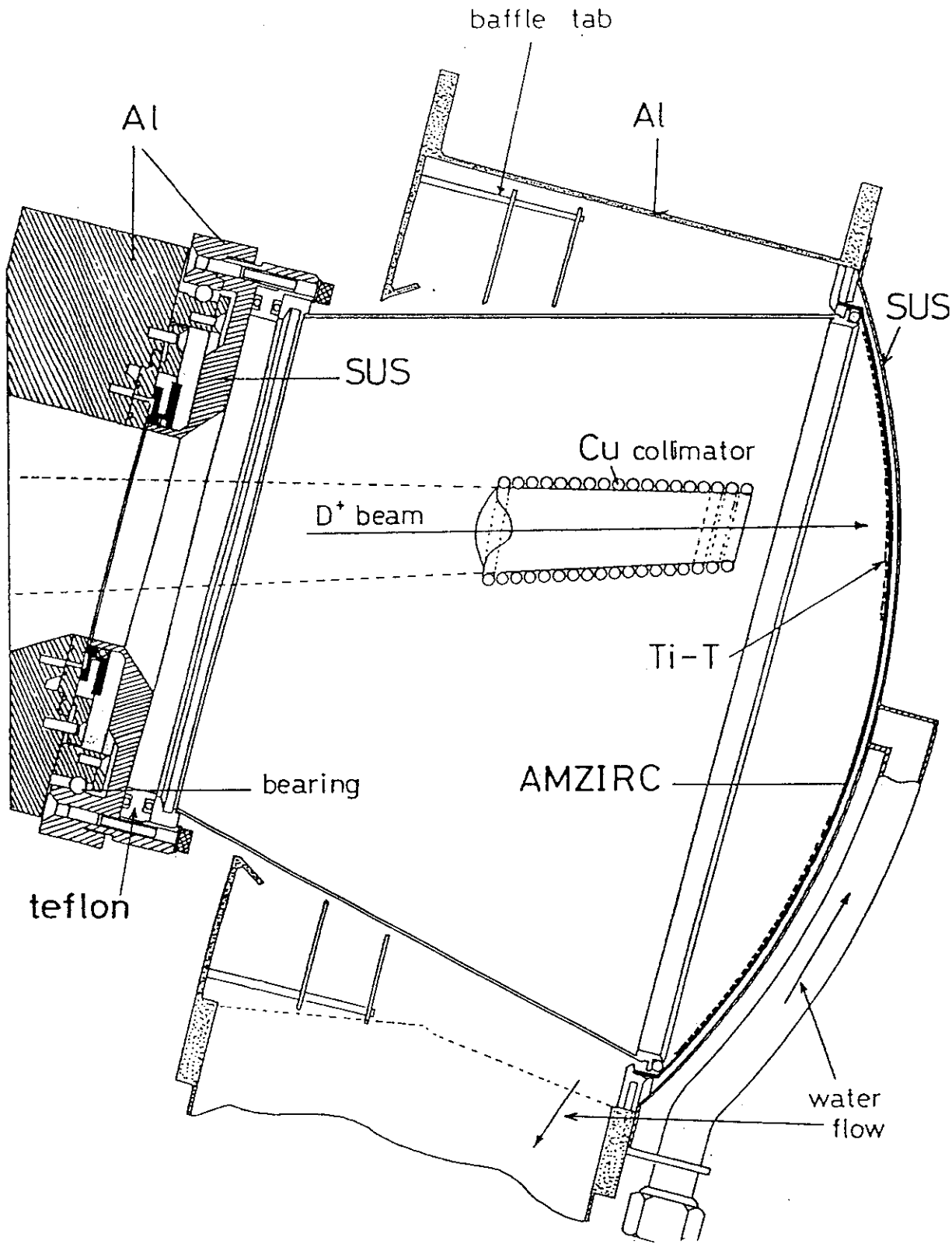

Fig. 1 Vertical Cross Section of the Target Assembly

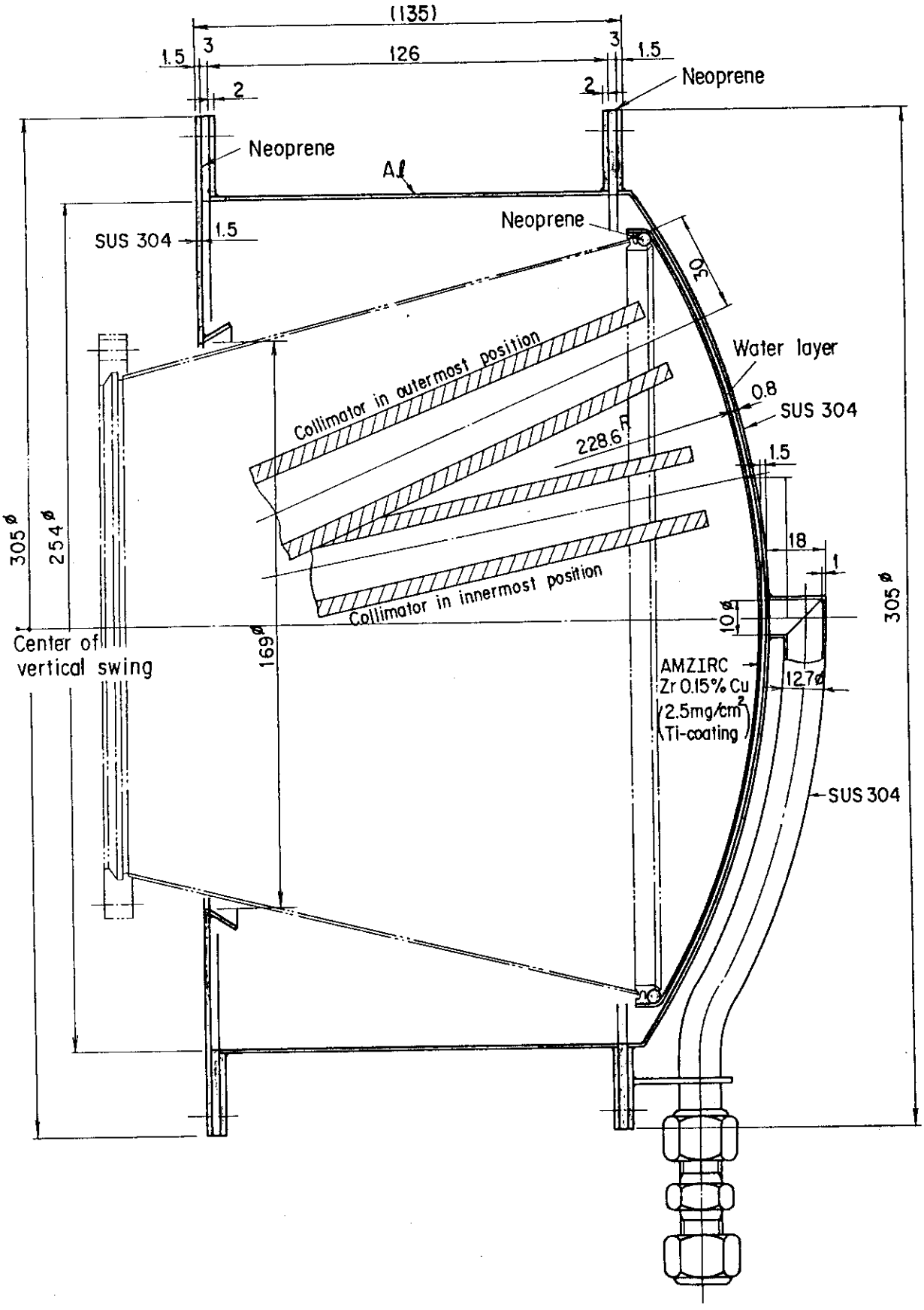

Fig. 2 Detailed Configuration of the Cover Section

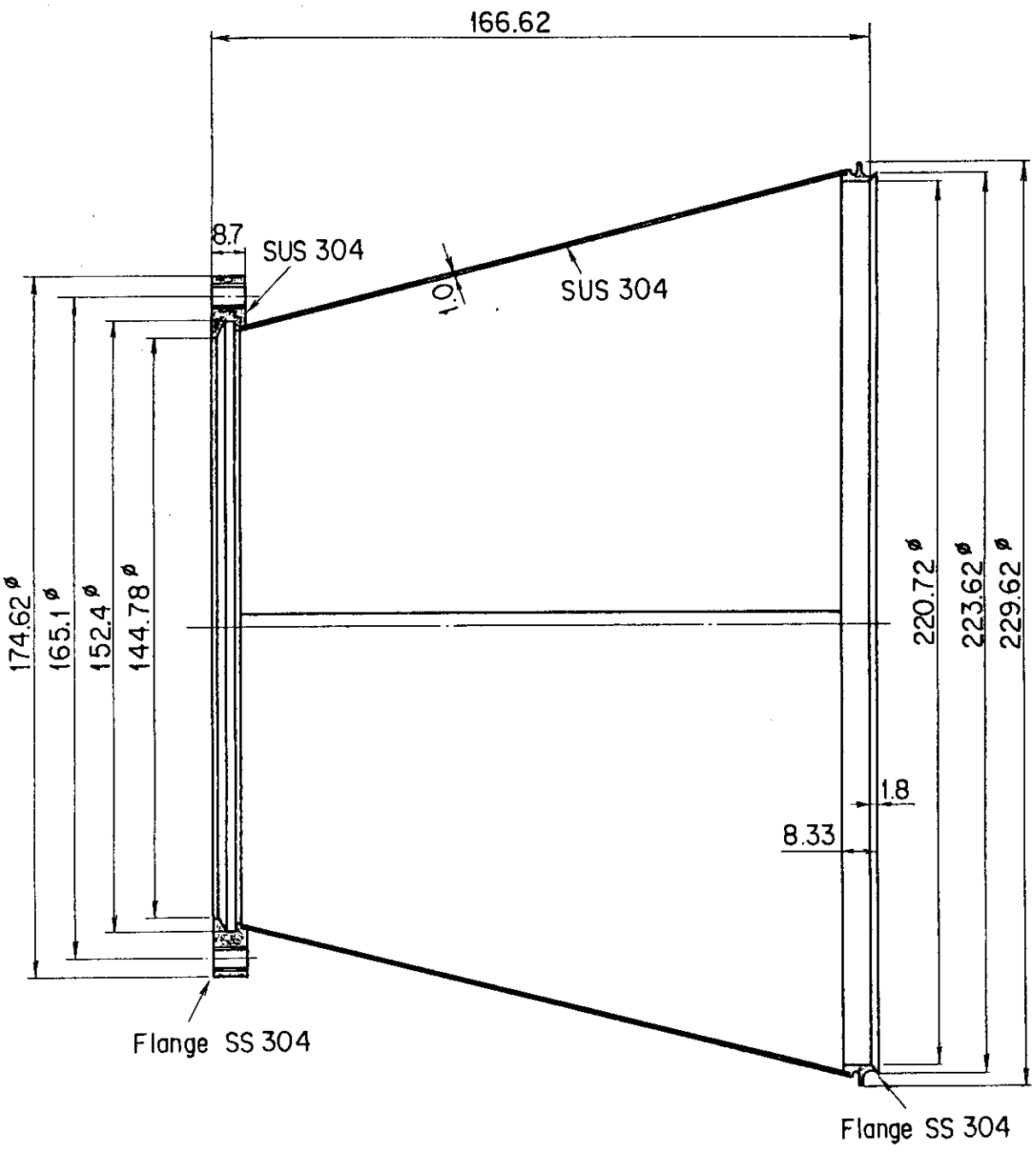

Fig. 3 Detailed Configuration of the Rotating Cone Section

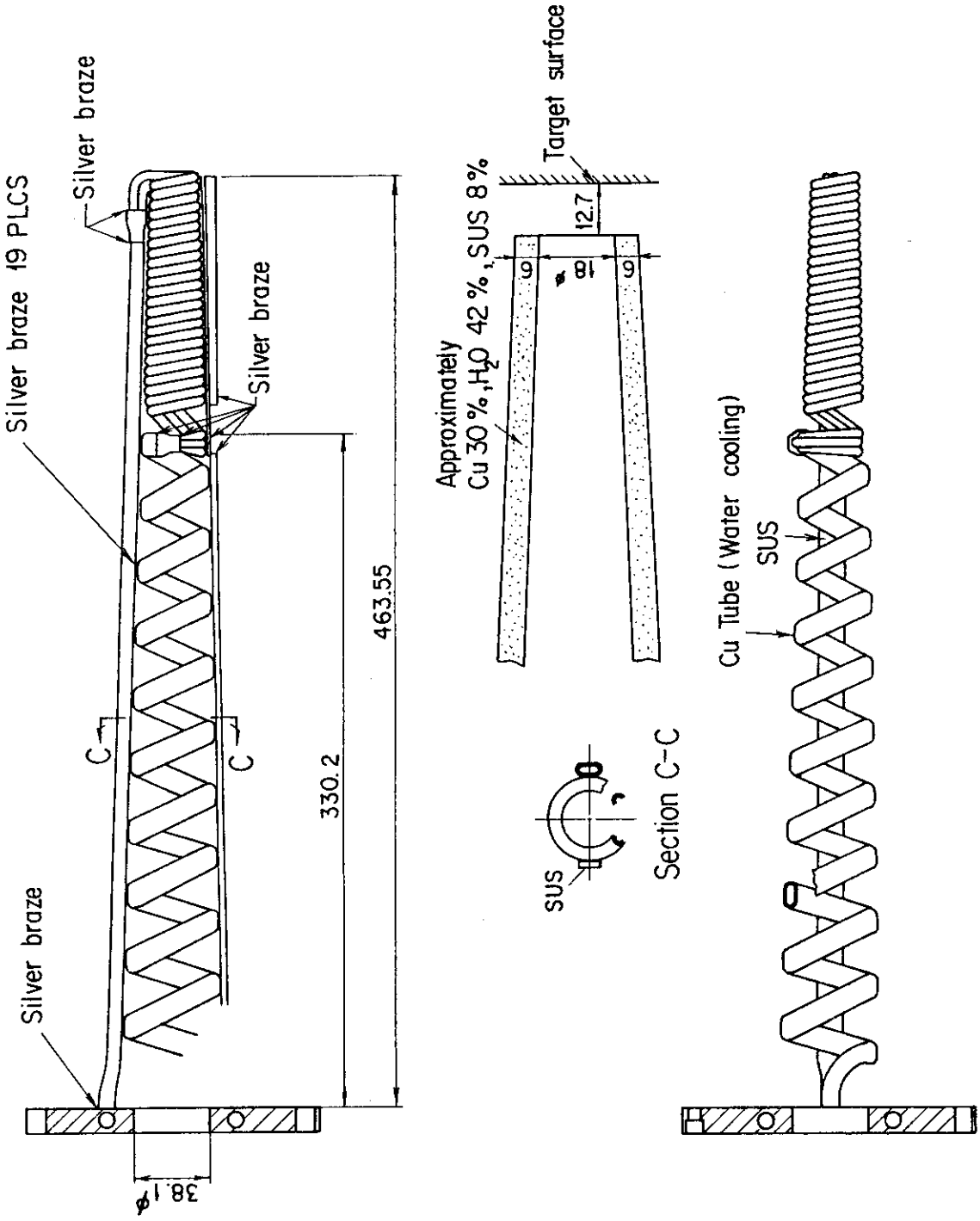

Fig. 4 Detailed Configuration of the Beam Collimator and Its Calculational Model.

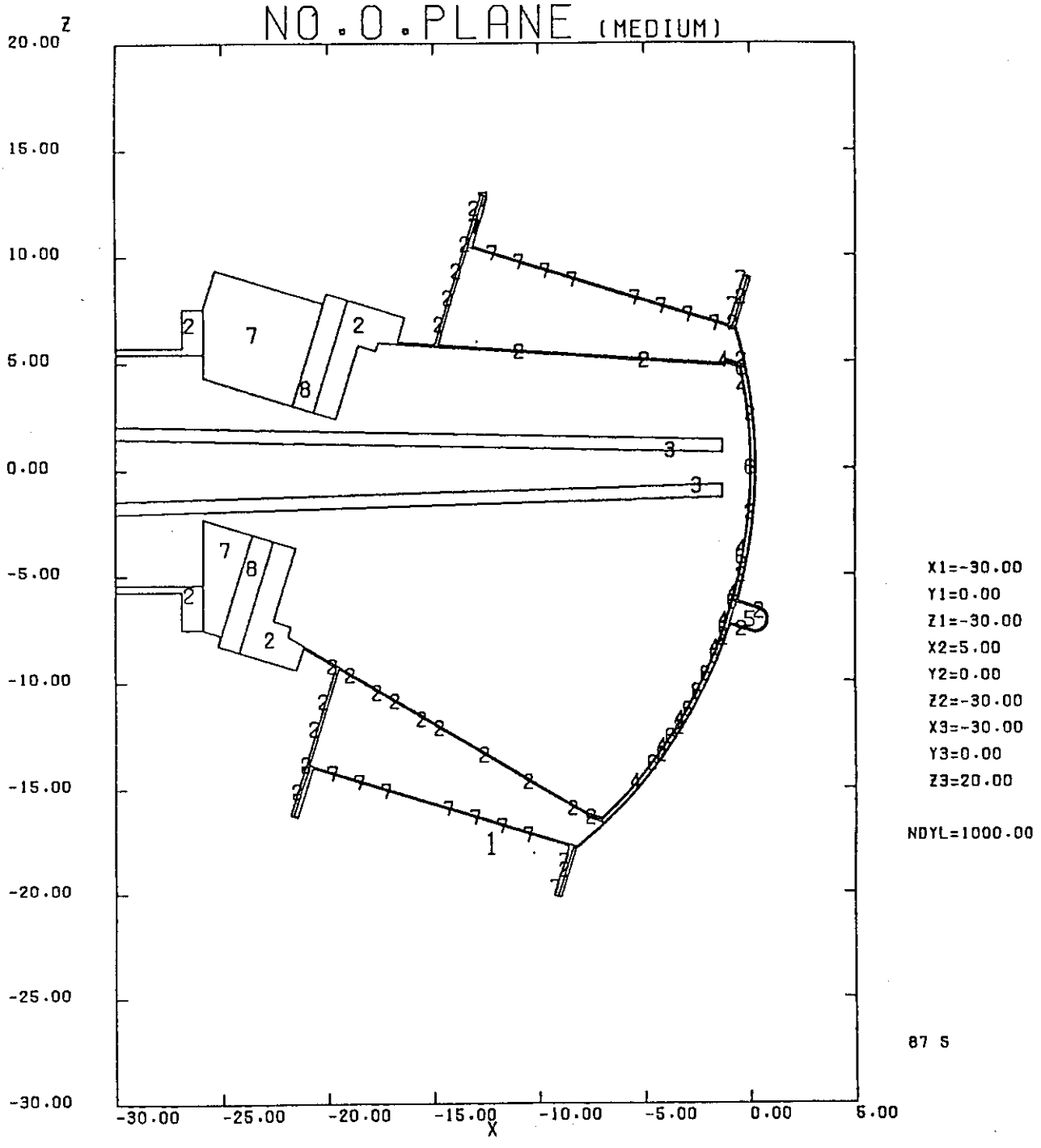

Fig. 5a Vertical Cross section of the Calculational Model of the Target Assembly. The numbers in the figure correspond to media as follows: 1 Air, 2 SUS 304, 3 Copper Tube, 4 Neoprene, 5 Water, 6 AMZIRC, 7 Aluminum (100% density), 8 Aluminum (50% Density).

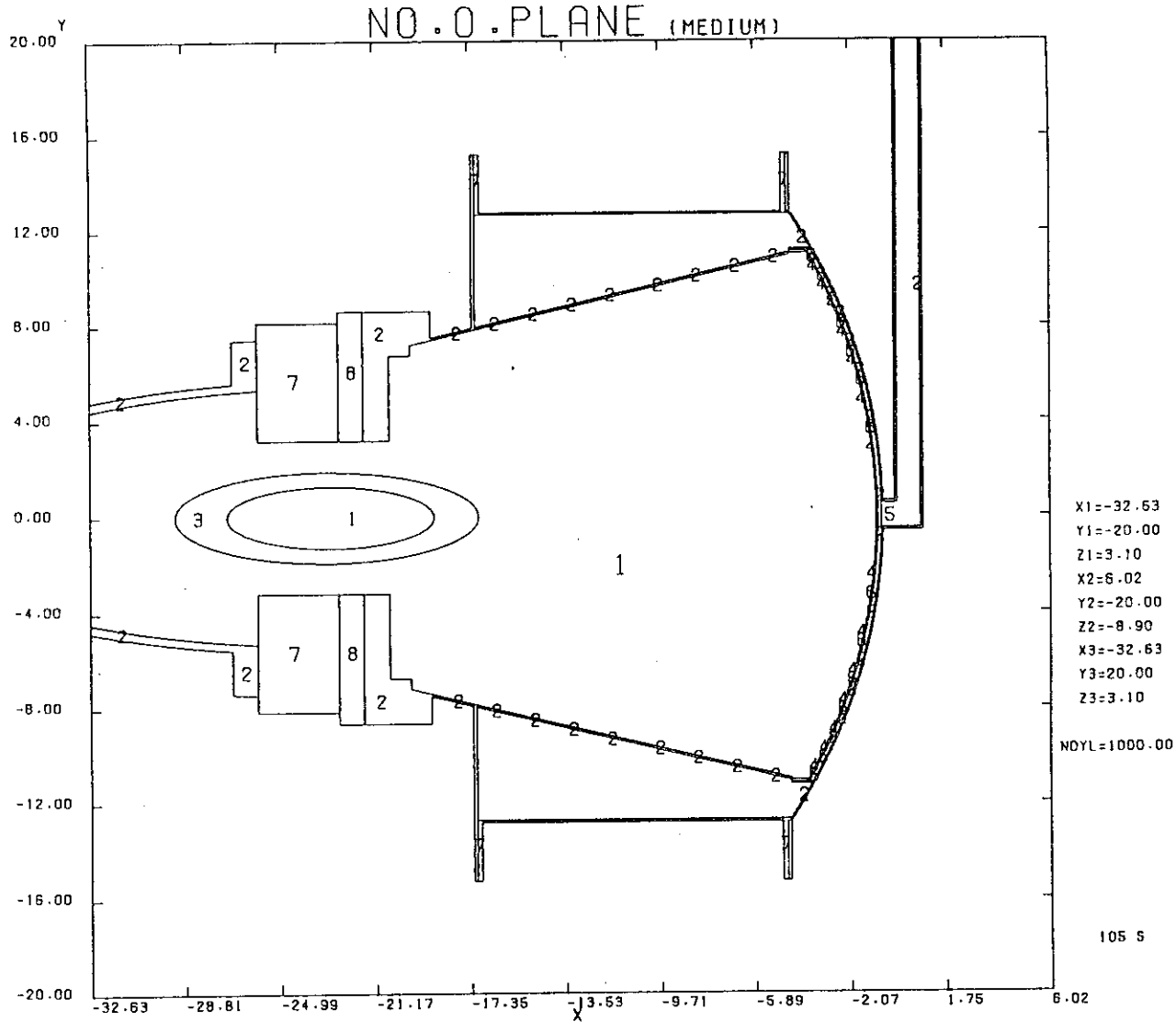

Fig. 5b Cross sectional View of the Calculational Model of the Target Assembly along the Axis of Rotation. The numbers in the figure correspond to media as follows: 1 Air, 2 SUS 304, 3 Copper Tube, 4 Neoprene, 5 Water, 6 AMZIRC, 7 Aluminum (100% density), 8 Aluminum (50% density).

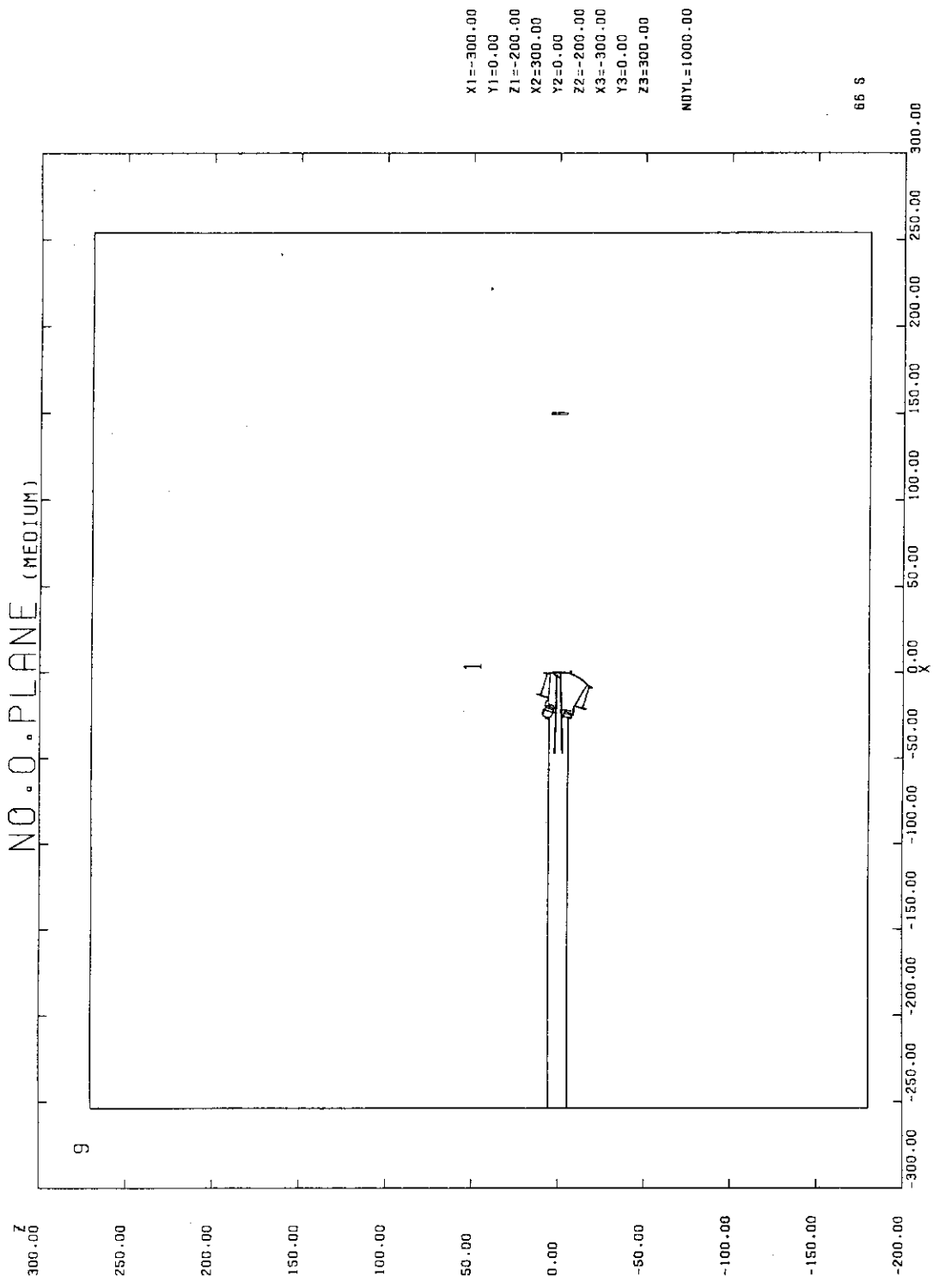

Fig. 6 Vertical Cross Section of the Target and the Room. The number in the figure correspond to media as follows: 1 Air, 9 Room Wall Concrete.

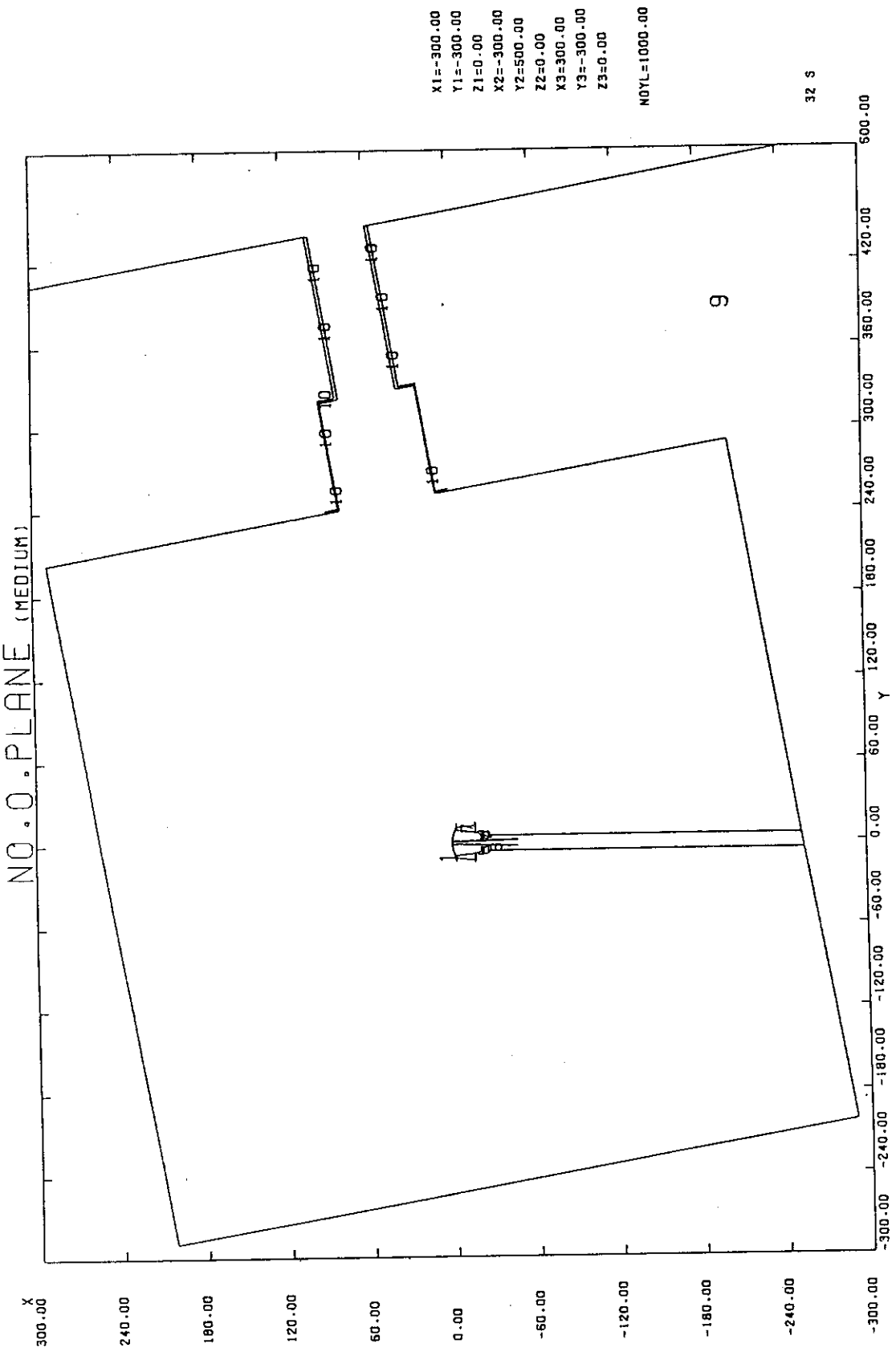

Fig. 7 Horizontal Cross Section of the Target and the Room. The number in the figure correspond to media as follows: 1 Air, 9 Room Wall Concrete, 10 Iron.

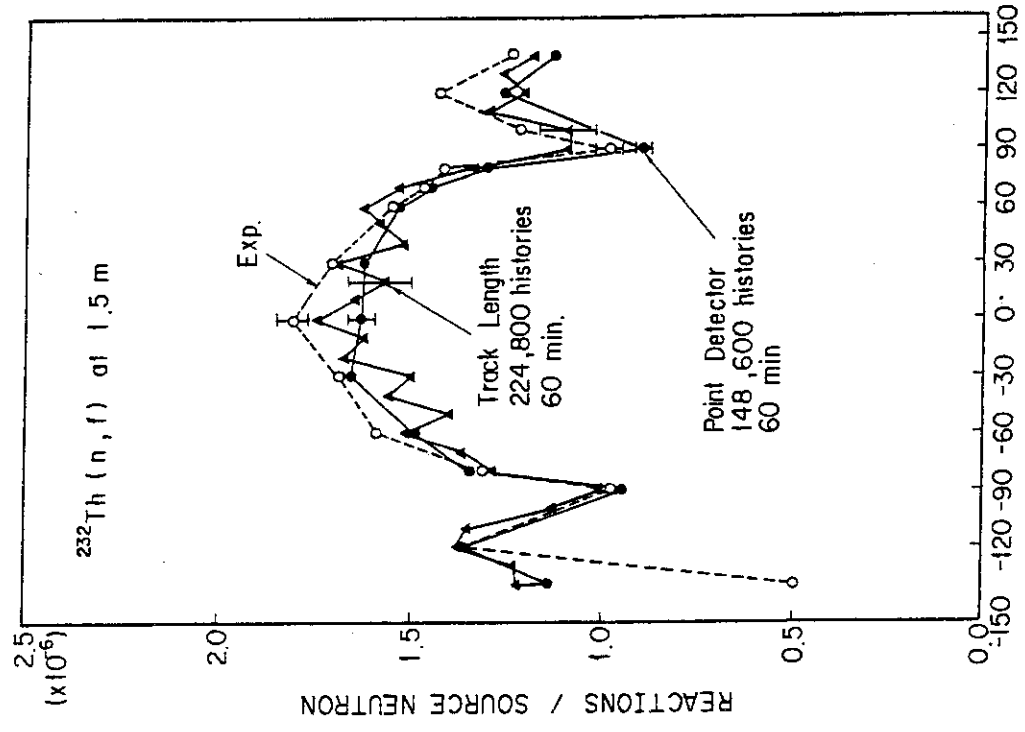

Fig. 9 Angular Distribution of ^{232}Th Fission Rate

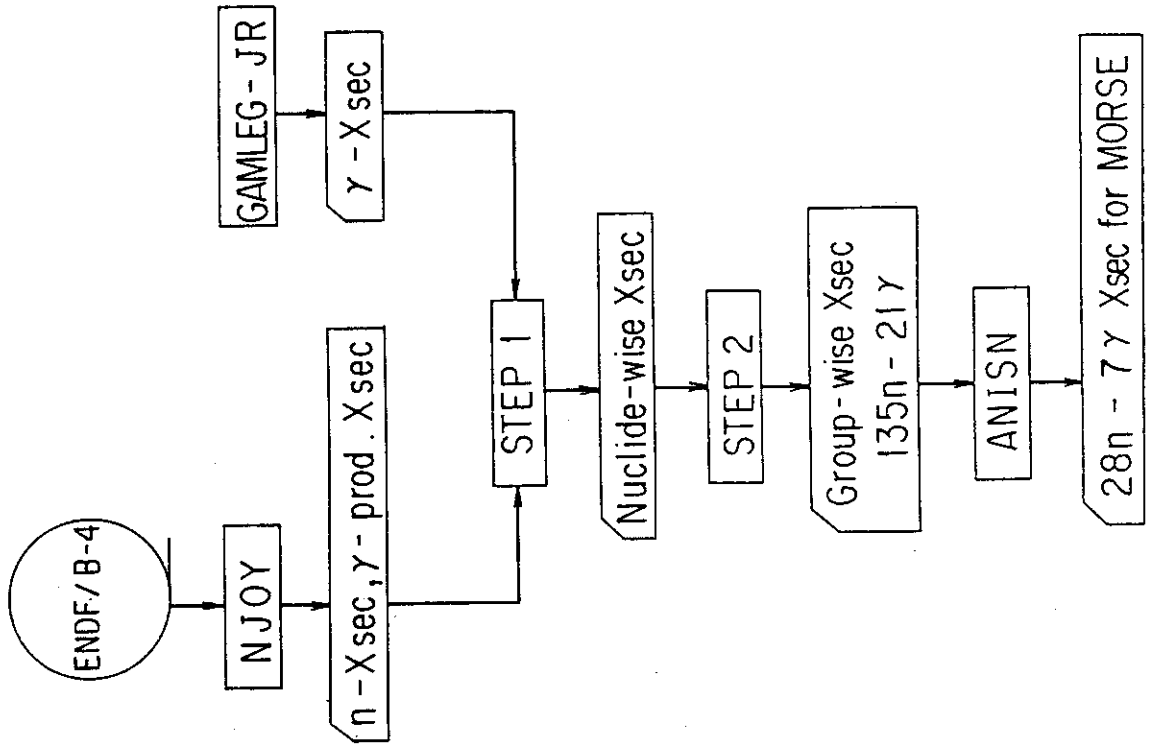

Fig. 8 Calculational Flow for the Macroscopic Cross Section Production

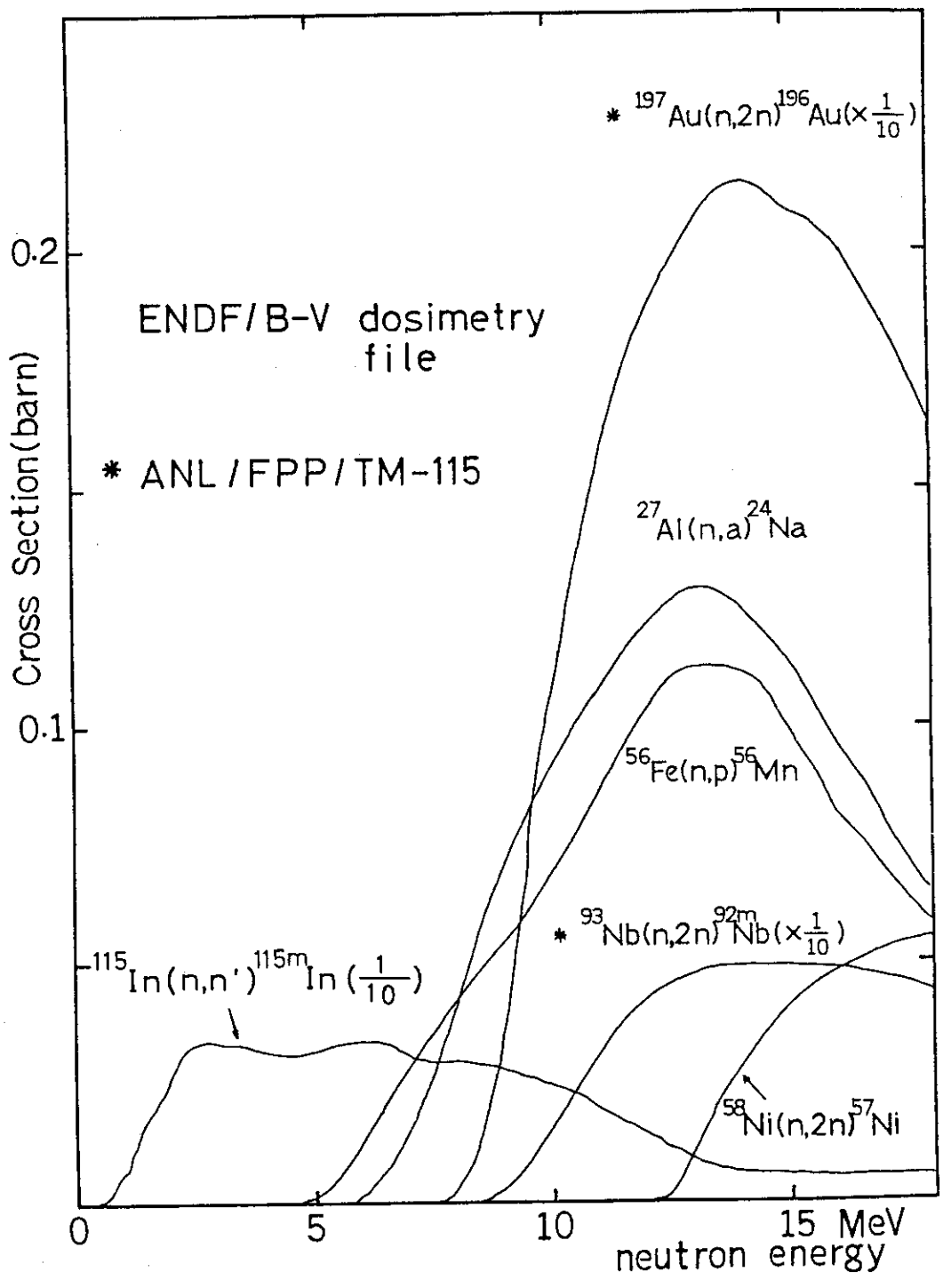

Fig.10a Cross Sections of the 6 Threshold Reactions

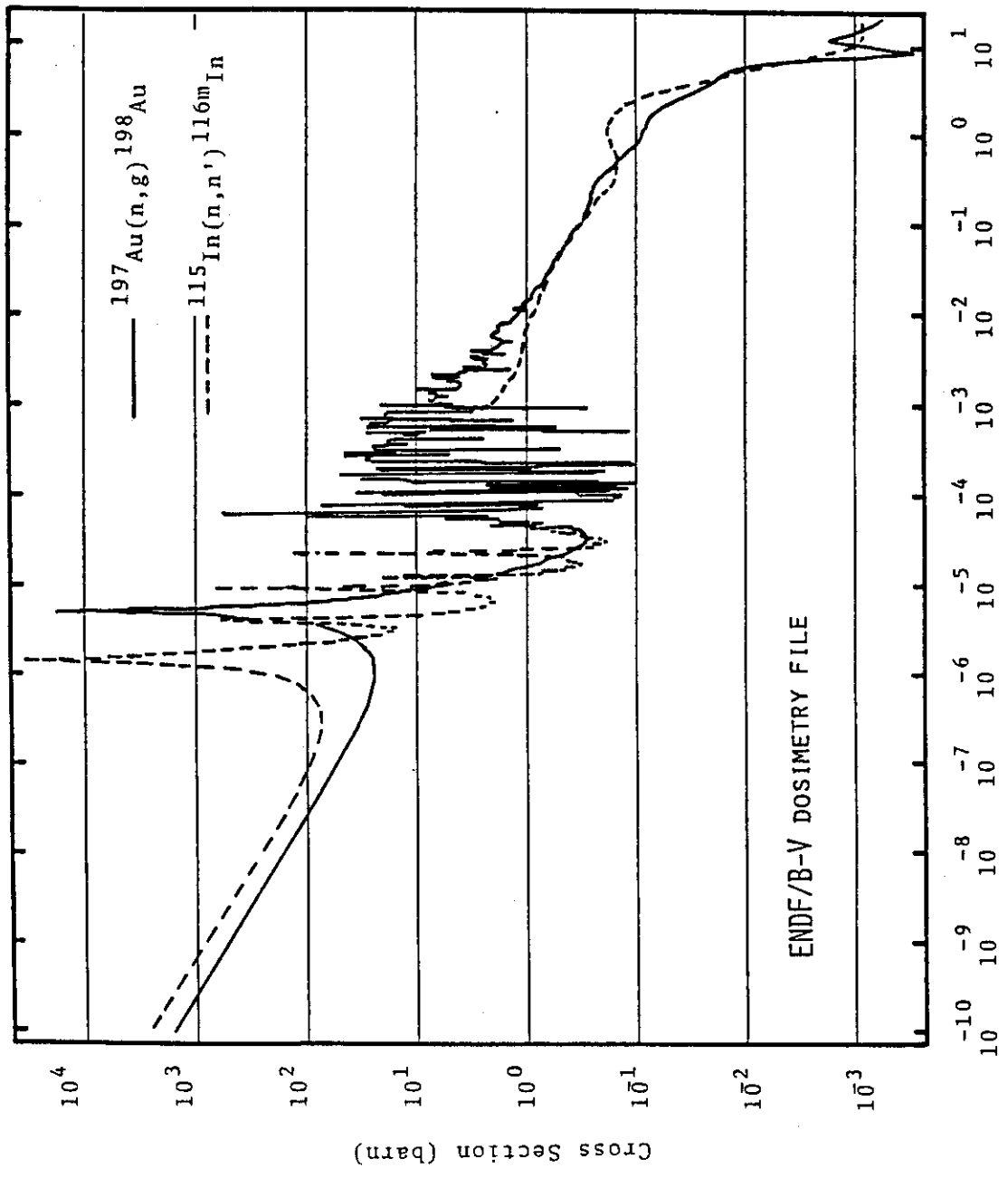

Fig.10b Cross Sections of the 2 (n,γ) Reactions

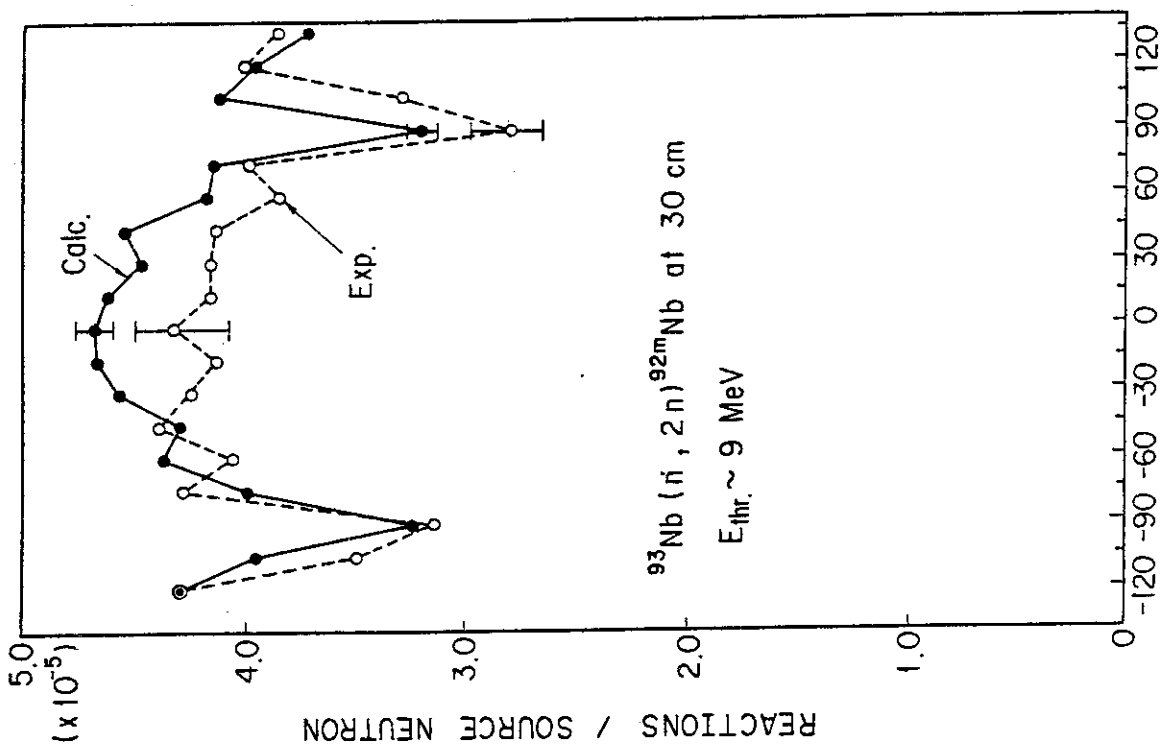

Fig.12 Angular Distribution of ^{93}Nb(n,2n)^{93m}Nb Reaction Rate

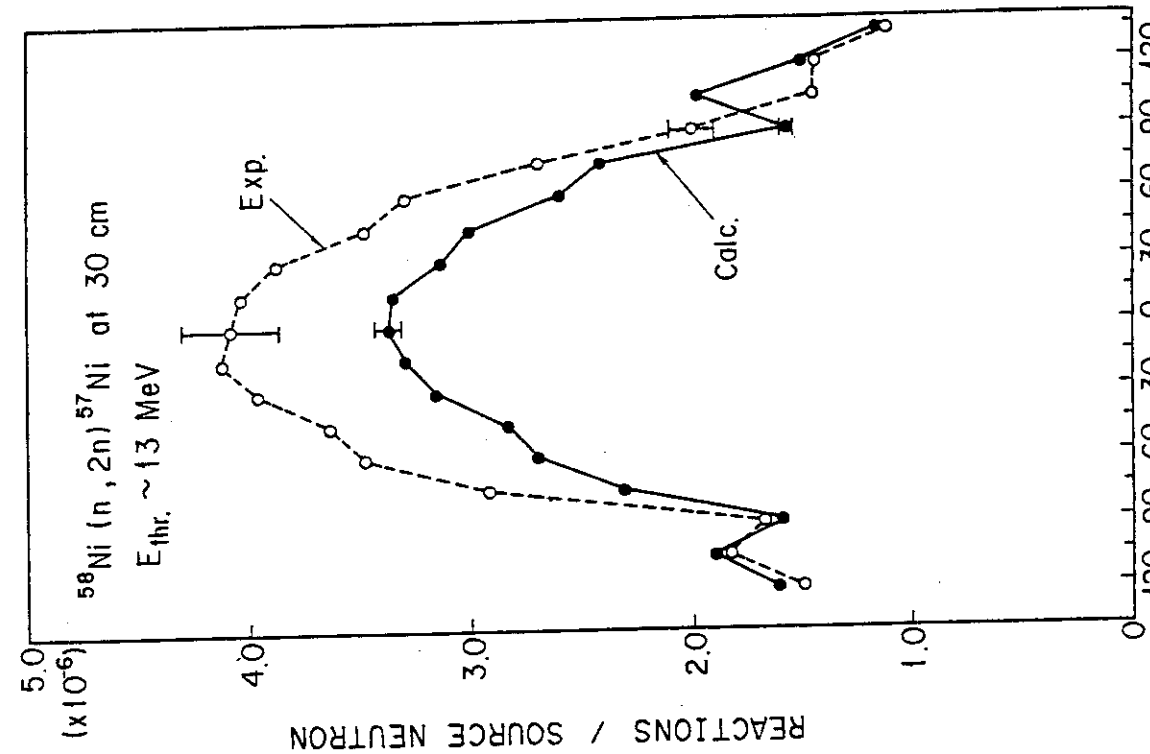

Fig.11 Angular Distribution of ^{58}Ni(n,2n)^{57}Ni Reaction Rate

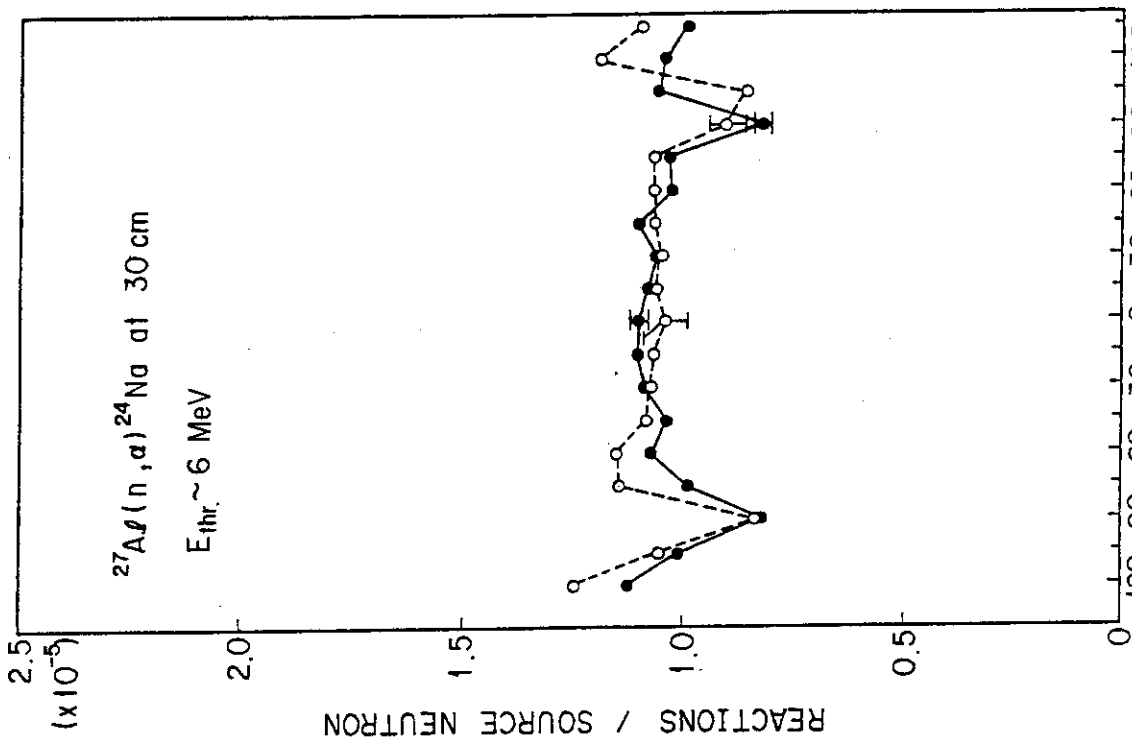

Fig.14 Angular Distribution of $^{27}Al(n,\alpha)^{24}Na$ Reaction Rate

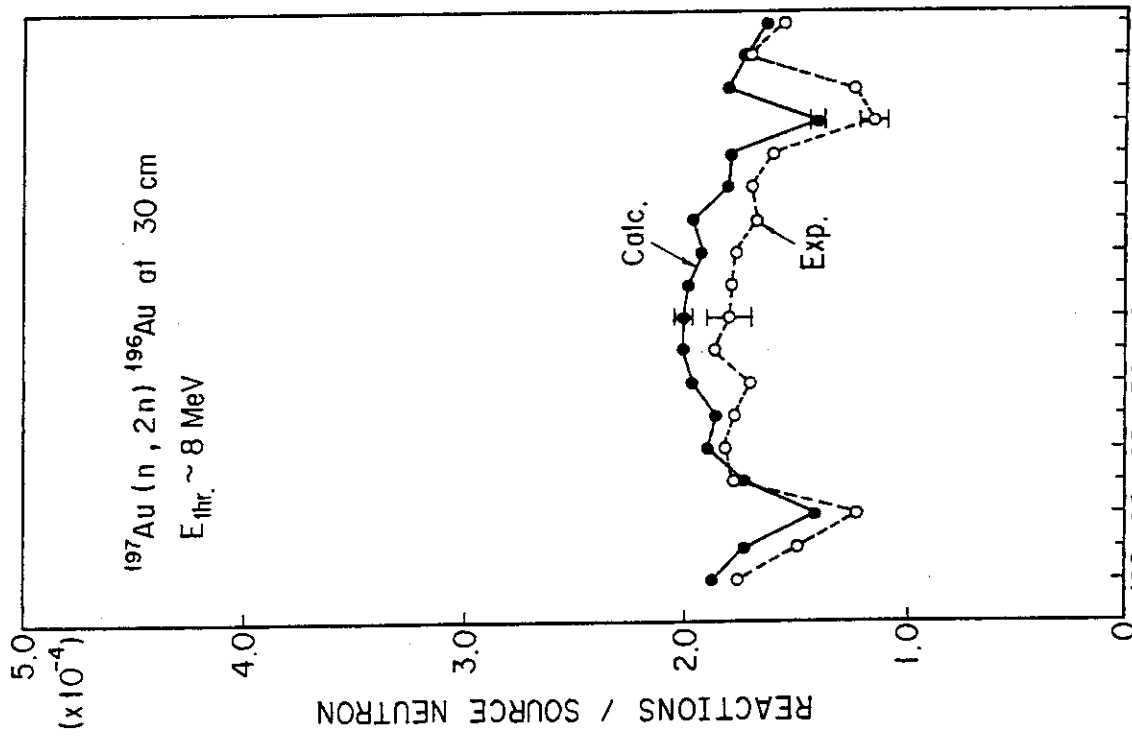

Fig.13 Angular Distribution of $^{197}Au(n,2n)^{196}Au$ Reaction Rate

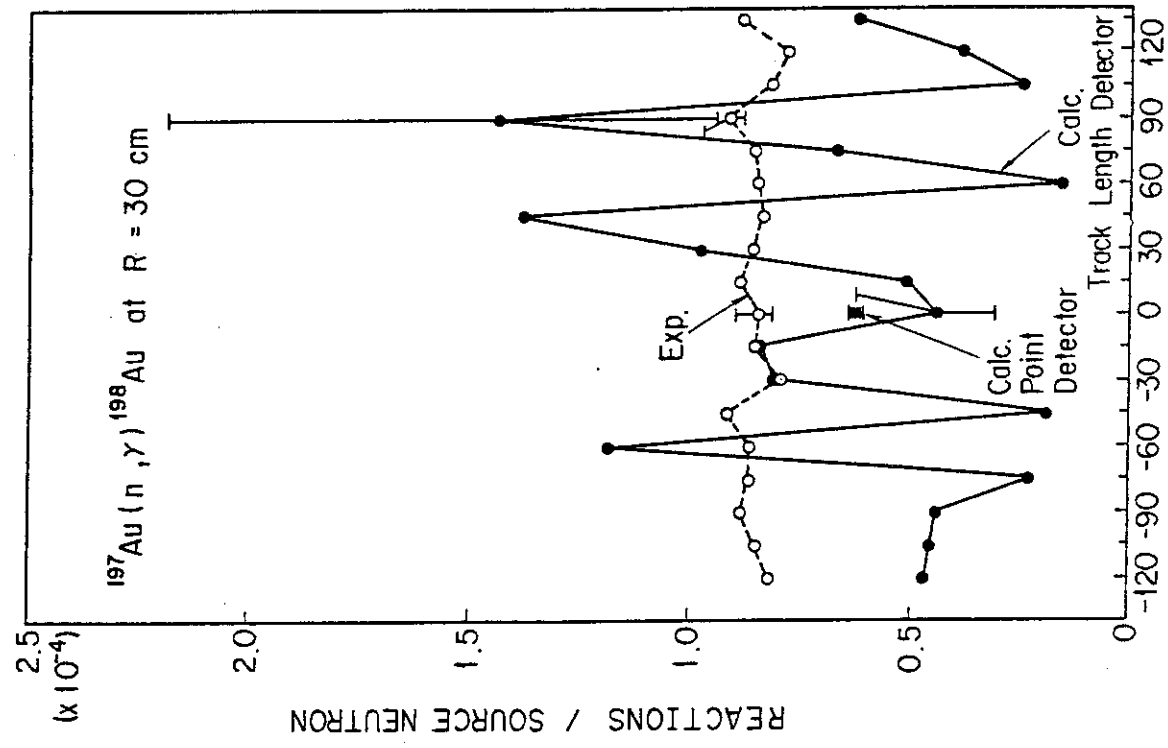

Fig.16 Angular Distribution of $^{197}Au(n,\gamma)^{198}Au$ Reaction Rate

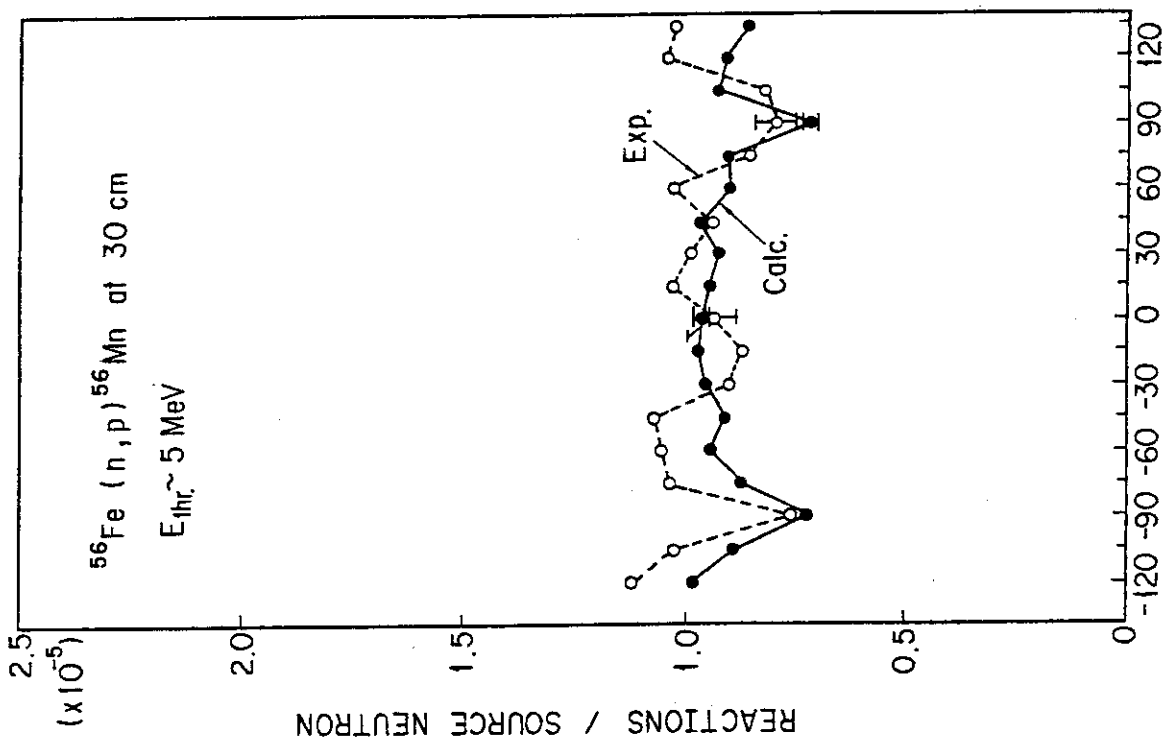

Fig.15 Angular Distribution of $^{56}Fe(n,p)^{56}Mn$ Reaction Rate

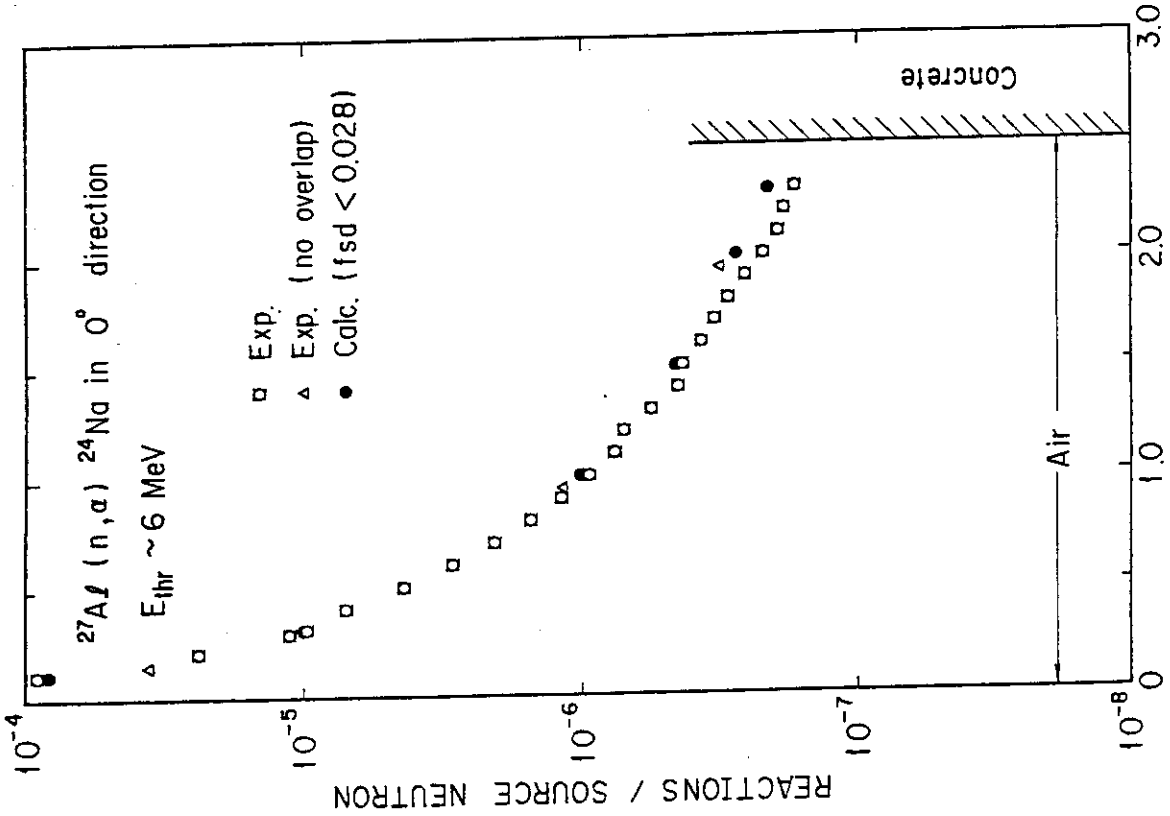

Fig.18 Radial Distribution of $^{27}Al(n,\alpha)^{24}Na$ Reaction Rate

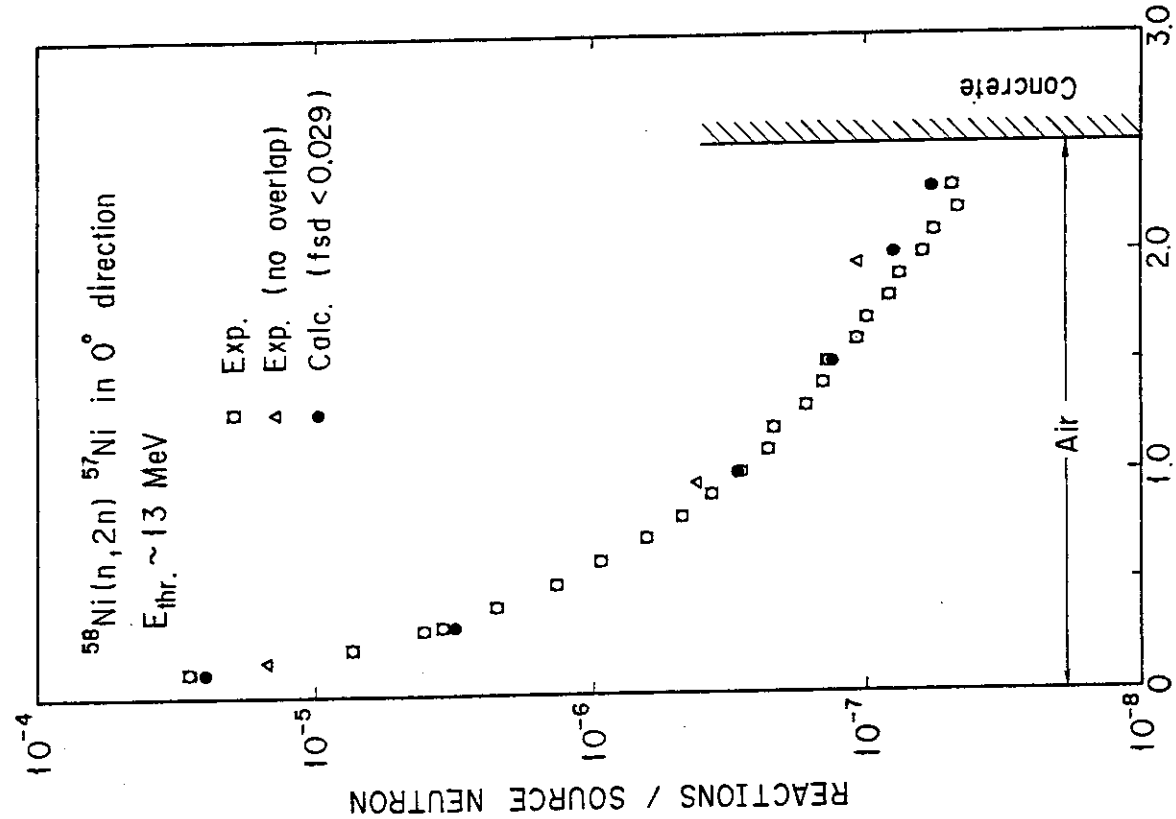

Fig.17 Radial Distribution of $^{58}Ni(n,2n)^{57}Ni$ Reaction Rate

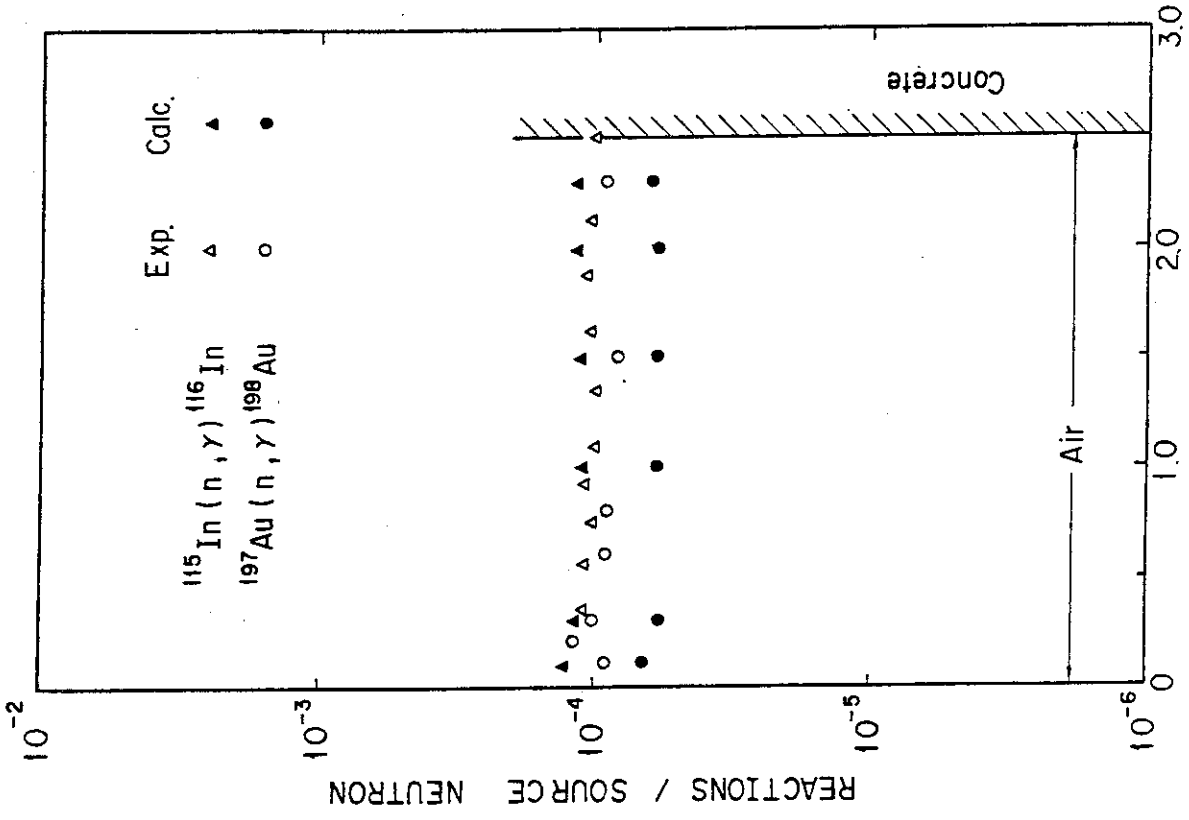

Fig.20 Radial Distribution of $^{115}In(n,\gamma)^{116}In$ and $^{197}Au(n,\gamma)^{198}Au$ Reaction Rate

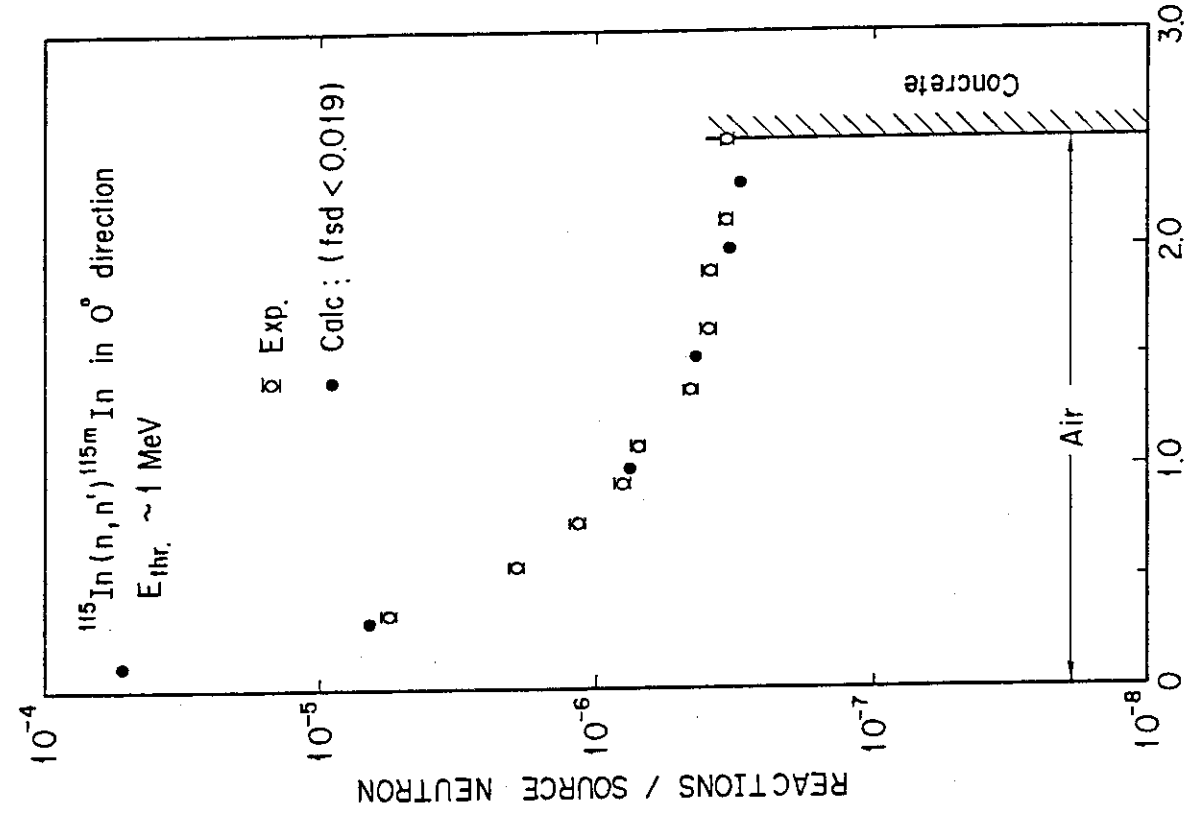

Fig.19 Radial Distribution of $^{115}In(n,n')^{115m}In$ Reaction Rate

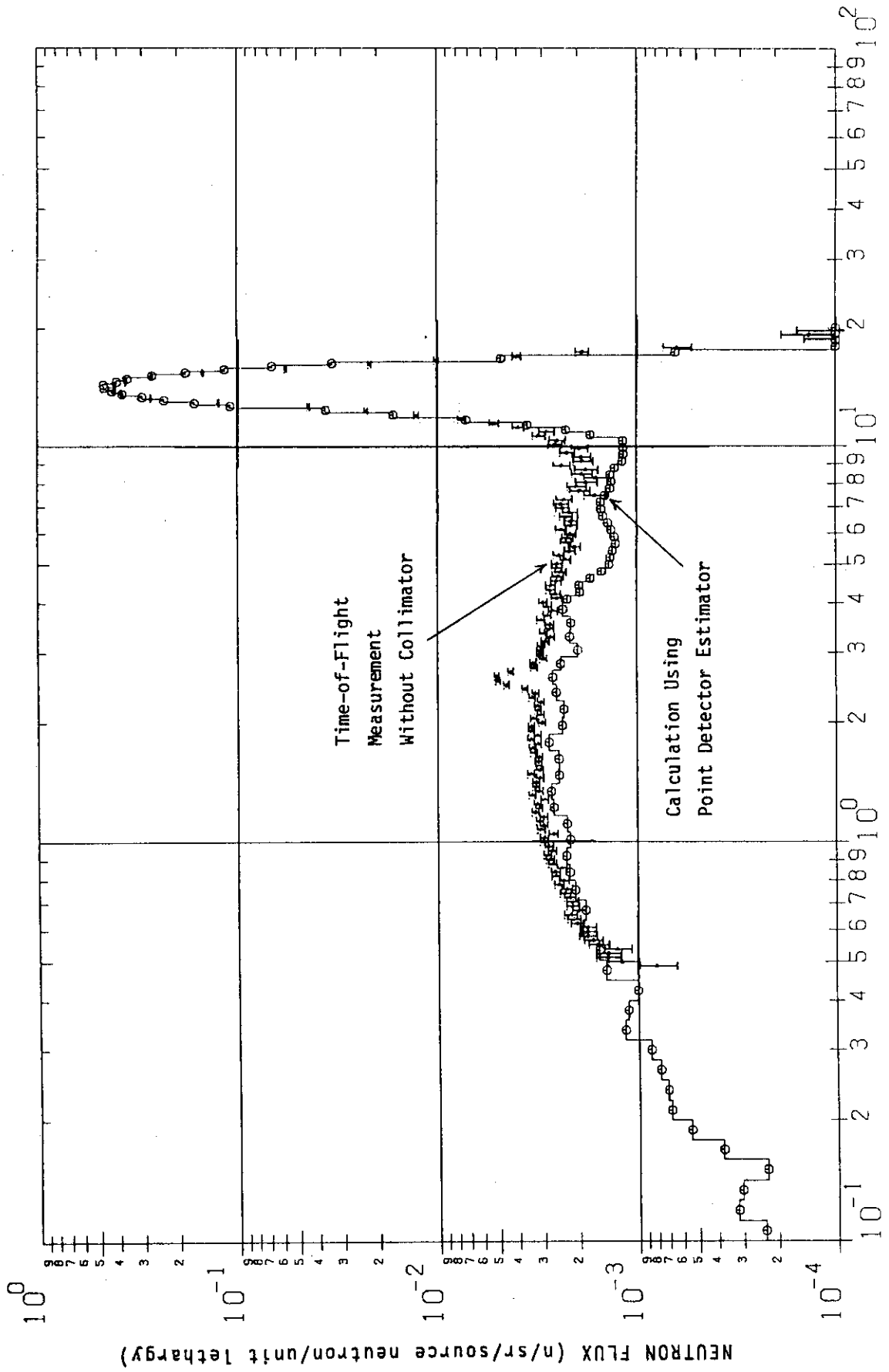

Fig.21 Source Neutron Spectrum in the 80° Direction